Core level and valence band photoemission spectra of Au clusters embedded in carbon

K. Takahiro,[a] S. Oizumi, A. Terai, and K. Kawatsura
Department of Chemistry and Materials Technology, Kyoto Institute of Technology, Matsugasaki, Sakyo, Kyoto 606-8585, Japan

B. Tsuchiya and S. Nagata
Institute for Materials Research, Tohoku University, 2-1-1 Katahira, Aoba, Sendai 980-8577, Japan

S. Yamamoto
Quantum Beam Science Directorate, Japan Atomic Energy Agency, 1233 Watanuki, Takasaki, Gunma 370-1292, Japan

H. Naramoto and K. Narumi
Advanced Science Research Center, Japan Atomic Energy Agency, 1233 Watanuki, Takasaki, Gunma 370-1292, Japan

M. Sasase
The Wakasa-wan Energy Research Center, 64-52-1 Nagatani, Tsuruga, Fukui 914-0192, Japan

(Received 14 January 2006; accepted 1 August 2006; published online 30 October 2006)

X-ray photoelectron spectroscopy (XPS) has been applied for size estimation of Au clusters formed by ion implantation into glassy carbon. The 4*f* and 5*d* XPS spectra reveal the presence of the cluster 0.7–2.5 nm in diameter, depending on the Au concentration. The relationship between XPS 4*f*-binding energy shift and 5*d* splitting is determined for the Au clusters embedded in the carbon and found to be significantly different from the previous data for the ones supported on a carbon substrate. We suppose that this difference results from the effect of the environment around a cluster on Coulomb charging during photoemission at the final state. © *2006 American Institute of Physics*. [DOI: 10.1063/1.2359688]

I. INTRODUCTION

A nanometer-sized cluster, referred to as "nanocluster" hereafter, embedded in a matrix exhibits unusual optical,[1–3] electrical,[4,5] and magnetic[6,7] properties. A large number of methods, including cosputtering,[8,9] sequential evaporation,[10] sol-gel deposition,[11,12] and ion implantation,[13–15] have been applied for the preparation of nanoclusters in a matrix. Of these techniques ion implantation is very promising for the formation of nanoclusters because of its ability to control the type and concentration of the implanted atoms. In addition, ion implantation can be, in principle, applied for any combination of ions and matrices.

The size distribution of nanoclusters is a key parameter to control the properties of cluster-dispersed materials. Usually, implanted atoms as well as defects distribute nonuniformly along depth, resulting in the depth-dependent nucleation and growth of nanoclusters. It is, therefore, necessary to examine the depth-dependent size distribution of nanoclusters. Cross sectional transmission electron microscopy (XTEM) is often used to directly investigate their size. However, much effort and time have to be paid to prepare specimens for XTEM observation. Furthermore, for very small clusters of subnanometer size, XTEM is mostly unable to measure their size.

Alternatively, x-ray photoelectron spectroscopy (XPS) can be used to estimate the size of nanoclusters. It is known that the core level binding energy of nanoclusters shifts toward higher energy from a bulk value, depending on their size. In particular, for Au nanoclusters *supported on* poorly conducting materials such as amorphous carbon and SiO_2, the relationship between Au 4*f*-binding energy shift and cluster size has been well established.[16–18] In our previous study,[19] XPS core level binding energies were measured for Au and Ag nanoclusters embedded in glassy carbon (GC) to estimate their size. A question arises, however, as to whether the above relationship is applicable to the nanoclusters *embedded in* GC.

The XPS binding energy shifts for clusters arise mainly from Coulomb charging of a cluster during photoemission.[20–24] Therefore the environment of the cluster affects the charging itself. In addition, the interaction of the charged cluster with the outgoing photoelectron depends on the nature, e.g., dielectric constant, of the surrounding materials. Very recently, Imamura and Tanaka[25] showed that the binding energy shift due to Coulomb charging changed with the strength of nanocluster-substrate interaction for alkanethiolate-passivated Au nanoclusters on graphite substrates. The XPS binding energy shifts, therefore, would be sensitive to the surroundings. By contrast, the spin-orbit energy splitting in a valence band level, which is essentially insensitive to the surroundings, can be a measure of the size of nanoclusters if the charge transfer between the cluster and surroundings is negligibly small. In an XPS Au 5*d* valence band spectrum, for example, $5d_{5/2}$ and $5d_{3/2}$ levels are well

[a]Also at II. Institute of Physics, University of Göttingen, Friedrich-Hund-Platz 1, 37077 Göttingen, Germany; electronic mail: takahiro@kit.ac.jp

separated for a bulk material,[26,27] and the splitting between $5d_{5/2}$ and $5d_{3/2}$ decreases as the size of a Au nanocluster decreases.[16,20,28–34]

In this work, the $4f$-binding energy shift as well as the $5d$ splitting were simultaneously measured on Au nanoclusters embedded in GC. The relationship between $4f$-binding energy shift and $5d$ splitting, referred to as the $4f$ shift-$5d$ splitting relation, enables us to clarify whether the relationship between the $4f$-binding energy shift and cluster size, referred to as the $4f$ shift-size relation, which has been obtained for isolated clusters, is valid or not for embedded clusters. In the present study, the validity of the $4f$ shift-size relation for Au nanoclusters embedded in a matrix is examined. When the present $4f$ shift-$5d$ splitting relation coincides with the previous one for isolated clusters, the $4f$ shift-size relation is applicable to the size estimation of the embedded clusters. The carbon matrix is chosen because no sample charging effect during XPS is expected and the interaction between Au and C atoms, i.e., chemical shift, is negligible. Moreover, the valence band of amorphous carbon is very weak and flat over the energy range of 0–10 eV, on which the Au $5d$ valence band lines appear.

II. EXPERIMENT

Glassy carbon (Tokai Carbon, Japan; GC-30 grade) was mechanically polished to a mirror surface with 1 μm diamond slurry on a cloth lap. The GC was implanted with 500 keV Au^+ ions to a fluence of $1\times10^{17}/cm^2$. Au implantation was performed using a tandem accelerator from the Institute for Materials Research (IMR) of Tohoku University. The depth distributions of implanted atoms were analyzed by using Rutherford backscattering spectrometry (RBS) with 2 MeV He ions from a single-end accelerator from Takasaki Ion Accelerators for Radiation Application (TIARA) of the Japan Atomic Energy Agency. The projected range of the Au ions estimated by RBS was approximately 255 nm, assuming that the density of the GC matrix was 1.5 g/cm^3. Au nanoclusters were detected in a GC matrix by glancing angle (2° with respect to the surface) incidence x-ray diffraction, and their average size was estimated to be 2–3 nm using Scherrer's equation.[35,36]

XPS using nonmonochromatized Mg $K\alpha$ radiation ($h\nu$ =1253.6 eV) was performed with JEOL 9010. The $4f$ core level and $5d$ valence band spectra were taken with an analyzer pass energy of 10 eV. An inelastic background was subtracted using the Shirley method,[37] which was available in the software (SPECXPS) attached to the XPS system. The energy calibration to determine the work function of a spectrometer was made using polycrystalline Au, Ag, and Cu samples. To obtain the depth profile of XPS binding energies for the implanted Au, the surface of the implanted GC was etched with 0.8 keV Ar ions from a sputter etching gun equipped with JEOL 9010. The etching rate was determined to be 0.29 nm/s by the Au depth profile obtained from RBS. In XPS, the uncertainty for binding energy measurements was checked by the position of C $1s$ and Ar $2p$ lines and was estimated to be ±0.07 eV.

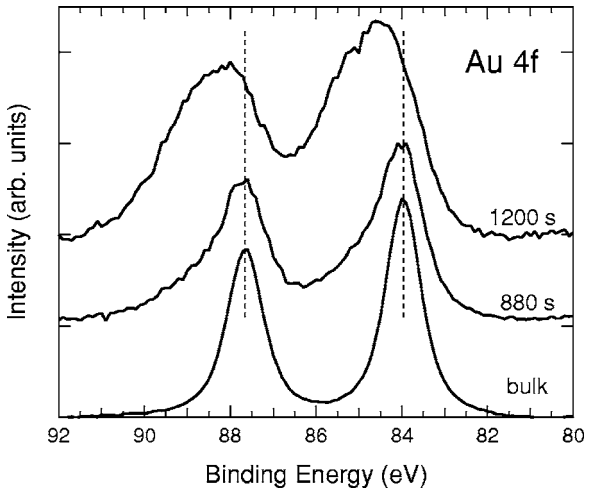

FIG. 1. Au $4f$ core level XPS spectra obtained from implanted Au atoms after sputter etching for 880 and 1200 s together with the spectrum of a bulk Au sample. The dashed lines indicate the peak positions of the $4f_{7/2}$ and $4f_{5/2}$ levels at 84.0 and 87.7 eV, respectively, for the bulk sample.

III. RESULTS

Figure 1 shows typical Au $4f$ core level XPS spectra obtained from implanted Au atoms after sputter etching for 880 and 1200 s, corresponding to the analyzing depths of ~255 and ~350 nm and the Au concentrations of 10 and 2 at. %, respectively. The spectrum from a bulk Au sample is also shown for comparison. The dashed lines indicate the peak positions of the $4f_{7/2}$ and $4f_{5/2}$ levels at 84.0 and 87.7 eV, respectively, for the bulk sample. The peak positions of the $4f_{7/2}$ and $4f_{5/2}$ levels for 880 s etched GC are very similar to the bulk values. On the other hand, The peak positions for 1200 s etched GC shift towards higher binding energy by 0.6 eV compared to those for bulk Au. The energy shift is understood by the effect of an averaged coordination number or cluster size on core level binding energy.[16,20,31] The widths of the $4f$ lines of the spectra for the implanted Au are 1.8 and 2.5 eV at 880 and 1200 s, respectively, relatively larger than those for bulk Au (1.1 eV). Indeed, the linewidth for the nanocluster increases with a decrease in size, since the atoms involved in the nanocluster have various coordination numbers.[16,20,31,38] In addition to the above effect, the large broadening accompanied by an asymmetric line shape shown in Fig. 1 suggests the presence of small Au nanoclusters with various sizes[39] in the analyzing layers.

Figure 2 shows the Au $5d$ valence band XPS spectra obtained from the Au implanted GC and bulk Au. Implanted Au atoms are not detected for the GC etched for 1600 s. The dashed lines are the peak positions of the $5d_{5/2}$ and $5d_{3/2}$ levels at 3.6 and 6.2 eV, respectively, for the bulk sample. The broken line indicates the lower binding energy edge of the $5d_{5/2}$ band (or the top of the d band, in other words) at 2.2 eV for bulk Au. The $5d$ splitting between the $5d_{5/2}$ and $5d_{3/2}$ levels is significantly reduced in the case of implanted Au. In addition, the lower binding energy edge of the $5d_{5/2}$ band moves from 2.2 to 3.3 eV for the 1200 s etched sample. Such a large shift (1.1 eV) cannot be explained only by the Coulomb charging[20–24] of the Au clusters since the $4f$ shift is ~0.6 eV as seen in Fig. 1. In the spectrum of the

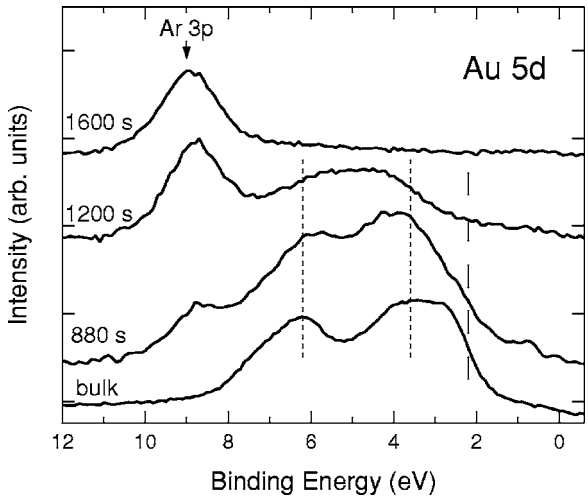

FIG. 2. Au 5*d* valence band XPS spectra obtained from implanted Au atoms after sputter etching for 880, 1200, and 1600 s together with the spectrum of a bulk Au sample. The dashed lines indicate the peak positions of the $5d_{5/2}$ and $5d_{3/2}$ levels at 3.6 and 6.2 eV, respectively, for the bulk sample. The broken line indicates the lower binding energy edge of the $5d_{5/2}$ band at 2.2 eV for the bulk Au.

1200 s etched sample, a prominent line of Ar 3*p* hinders the extraction of the width of the 5*d* splitting. In Fig. 3, each of the spectrum is decomposed into three Gaussian functions to determine the peak positions of the $5d_{5/2}$ and $5d_{3/2}$ levels. In the fitting, the linewidth of Ar 3*p* was fixed at 1.53 eV, and the intensity ratios of $5d_{5/2}$ to $5d_{3/2}$ were kept in the range of 1.3–1.4 for all spectra. The decomposition of the spectra reveals that the energy position of the $5d_{3/2}$ component remains almost unchanged, while the $5d_{5/2}$ one moves towards the lower binding energy. This tendency is consistent with the

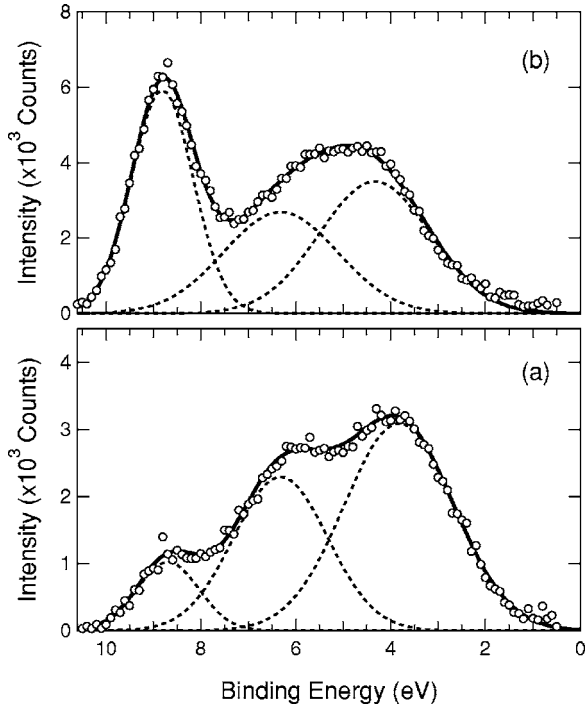

FIG. 3. The fitted Au 5*d* valence band XPS spectra for (a) 880 s and (b) 1200 s etched samples. The spectra are decomposed into three Gaussian functions.

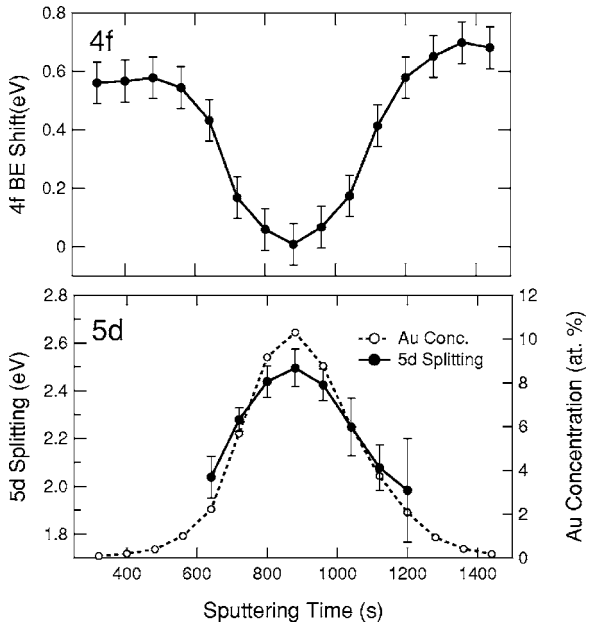

FIG. 4. The $4f_{7/2}$-binding energy shifts (upper panel) and 5*d* splittings (lower panel) as a function of etching time. The Au concentration profile is also shown in the lower panel.

previous works by Mason[31] and Bzowski *et al.*[32] for small Au clusters. The splittings between the $5d_{5/2}$ and $5d_{3/2}$ levels are determined to be 2.49±0.08 and 1.98±0.20 eV for the 880 and 1200 s etched GC samples, respectively. Furthermore, the widths of the 5*d* band for these samples are estimated to be 5.0 and 4.4 eV, significantly narrower than those for bulk Au (5.2 eV).

As seen in Figs. 1–3, the 4*f* and 5*d* spectra are remarkably different in their line shapes (including the peak position, linewidth, and splitting) from those of bulk Au, and depend on the etching time, i.e., depth. Etching-time dependence of the $4f_{7/2}$-binding energy shifts and 5*d* splittings is presented in Fig. 4 together with the Au concentration profile. It is found that the $4f_{7/2}$ shifts as well as 5*d* splittings are correlated strongly with the Au concentration. For etching times of 0–640 and 1100–1480 s, corresponding to the depths of 0–190 and 320–430 nm, in which the Au concentration is lower than 4 at. %, the $4f_{7/2}$-binding energy is shifted by 0.4–0.7 eV toward higher binding energy from a bulk value, and 5*d* splitting is ~2.0 eV. The larger $4f_{7/2}$ shift and smaller 5*d* splitting indicate that the size of Au cluster is smaller in these regions. DiCenzo *et al.*[16] experimentally determined the relationship between the Au 4*f*-binding energy shift as well as 5*d* splitting and average coordination number for the size selected Au clusters on a carbon substrate. Using their relationship, the 4*f*-binding energy shifts of 0.7 and 0.4 eV yield the average coordination numbers of 4 and 8 for Au cluster, corresponding to the sizes of 0.7 and 1.2 nm in diameter, respectively. On the other hand, the 5*d* splitting ~2.0 eV yields the average coordination number of ~8, consistent with the value obtained from the 4*f* shift. In these regions, this result suggests that the 4*f* shift-size relation used for Au clusters supported on a carbon substrate is applicable to the size estimation for Au clusters embedded in a carbon matrix. By contrast, for etching times of 720–1040 s,

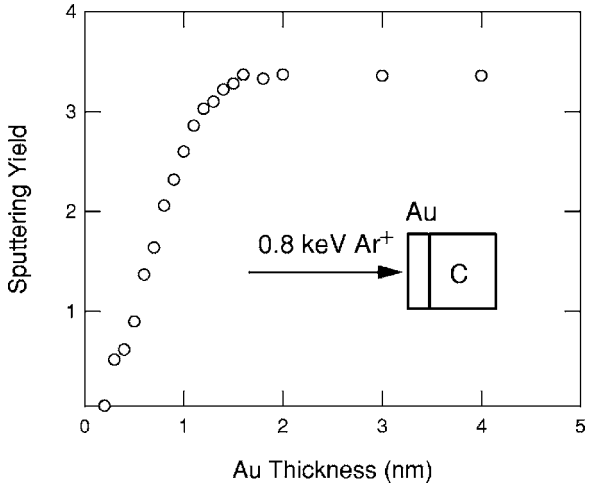

FIG. 5. Au thickness dependence of sputtering yield of Au for a Au/C bilayer calculated by the SRIM (Ref. 40).

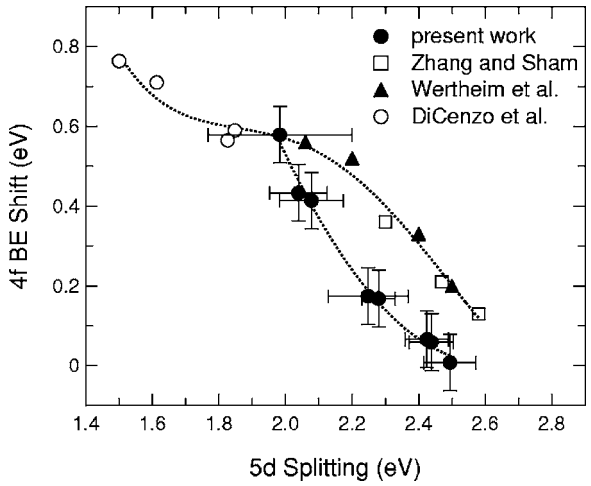

FIG. 6. The relationship between the $4f_{7/2}$-binding energy shift and $5d$ splitting for different types of Au nanoclusters, Au nanoclusters embedded in GC (full circles), thiol-passivated Au nanoclusters (Ref. 33) (open squares), thin Au films deposited on vitreous carbon (Ref. 20) (full triangles), and Au nanoclusters supported on amorphous carbon (Ref. 16) (open circles). The previous measurements (Refs. 16, 20, and 23) were performed using an Al $K\alpha$ radiation ($h\nu$=1486.6 eV). The dotted lines are drawn as a guide to the eyes.

corresponding to the depths of 210–300 nm and Au concentrations of 5.5–10 at. %, the $5d$ splitting of 2.2–2.5 eV yields the average coordination numbers of 9–10, corresponding to 1.5–2.5 nm, if the data of DiCenzo *et al.*[16] is interpolated, while the $4f_{7/2}$ shifts of 0–0.2 eV yield average coordination numbers larger than 10, corresponding to sizes larger than 2.5 nm in diameter. This discrepancy arises from the invalidity of the $4f$ shift-size relation for Au clusters embedded in a carbon substrate, considering that the previous $5d$ splitting-size relation should be valid since no charge transfer between Au and C is expected.

IV. DISCUSSION

In our experiment, sputter etching with 0.8 keV Ar ions was used to measure photoemission spectra of Au clusters embedded in GC. The sputter etching would change the size of Au clusters. However, the size modification by sputtering is not important for the comparison between the $4f$ shift and $5d$ splitting as discussed below. There may be a possibility that the sputter etching alters the environment of Au clusters; some of the Au cluster might reside on the surface due to a partial removal of the surrounding carbon. Sputtering yields of C and Au for 0.8 keV Ar incidence calculated using the SRIM (Ref. 40) are 0.16 and 3.4, respectively. Such a large difference in sputtering yields prevents the preferential sputtering of the surrounding carbon. The sputtering yield of Au clusters may be, however, reduced since the collision cascade is insufficiently developed inside the clusters. In order to clarify this, the cluster size dependence of the sputtering yield is simulated using a Au/C bilayer with various Au thicknesses, as shown in Fig. 5. The sputtering yield of a Au thin film gradually increases as the thickness increases and reaches the value of 3.4 at the thickness of 1.6 nm, suggesting that the sputtering yield of Au clusters with size larger than 1.6 nm is similar to that of bulk Au. Even for a Au thin layer of 0.3 nm thickness, the sputtering yield of Au is about three times larger than that of C. Most of the Au clusters formed in GC are, therefore, eroded faster than the surrounding C, which means that few Au clusters stay on the surface after the sputter etching. Thus, in XPS analysis together with the sputter etching, photoemission spectra are measured for Au clusters buried in the GC surface layer whose thickness corresponds to $4f$- or $5d$-electron mean free path of 3 nm.[41]

In the previous section, we found that the relationship between $4f_{7/2}$-energy shifts and cluster size, the $4f$ shift-size relation, was valid for smaller Au clusters of 0.7–1.2 nm, but invalid for larger Au clusters of 1.5–2.5 nm. In this section, we examine the relationship between $4f_{7/2}$ shift and $5d$ splitting, the $4f$ shift-$5d$ splitting relation, to discuss the validity of the $4f$ shift-size relation for Au clusters embedded in GC.

In Fig. 6, the measured $4f_{7/2}$-binding energy shifts are plotted as a function of $5d$ splitting. The previous data for Au nanoclusters deposited on carbon by DiCenzo *et al.*[16] and Wertheim *et al.*,[20] as well as thiol-passivated Au nanoclusters by Zhang and Sham,[33] are shown in this figure. Here the cluster size can be estimated by the $5d$ splitting. In previous cases, Au clusters are located on a substrate. Coulomb charging on Au nanoclusters during XPS analysis, i.e., $4f_{7/2}$-binding energy shift, may be affected by the electric conductivity σ of a substrate. In Refs. 16 and 20, amorphous carbon [$\sigma \sim 10^{-3}$ $(\Omega\ \mathrm{cm})^{-1}$ (Refs. 42–44)] and glassy carbon [$\sigma = 10^{2}$–10^{3} $(\Omega\ \mathrm{cm})^{-1}$ (Refs. 45–47)] were used, respectively. In the case of thiol-passivated Au nanoclusters, the electric conductivity of a substrate does not matter because they are decoupled with the substrate. It is noteworthy that a universal curve can be drawn for all the previous data, indicating that the $4f$ shift is insensitive to the electric conductivity of a substrate when Au clusters are supported on it. Boyen *et al.*[18] also showed that the $4f$ shift-size relation held for a variety of substrates.

It is evident that our data deviate from the previous one, especially in the $5d$ splitting range of 2.2–2.5 eV. As the $5d$ splitting is 2.5 eV, for example, corresponding to the size of ~2.5 nm in diameter, the $4f_{7/2}$ shift is ~0 eV in the present work, while ~0.2 eV in the previous work. We suppose that

this deviation results from a different environment of the Au nanocluster. In our case, Au nanoclusters ~2.5 nm in diameter are embedded in a carbon matrix. As a result, the positively charged core hole created via photoexcitation can be screened by conduction electrons of carbon on the time scale of a photoemission process, resulting in the smaller $4f$-energy shift. On the other hand, as mentioned above, for the $5d$ splitting of ~2.0 eV, corresponding to the size of ~1 nm in diameter, the $4f_{7/2}$-binding energy shifts in our work are very similar to those in the previous measurements. This implies that conduction electrons insufficiently screen the core hole in the Au nanocluster of ~1 nm. Thus our data and the earlier one are similar for the Au nanocluster of ~1 nm, but are significantly different for the larger cluster of 1.5–2.5 nm. Next, we discuss the reason for this size-dependent difference according to the environment of a Au nanocluster.

Au nanoclusters are formed when the Au concentration exceeds the solubility limit of Au in carbon by nucleation and growth. From the thermodynamic point of view, free volume, such as pore, void, and cavity, acts as a sink for migrating Au and then becomes a preferential nucleation site.[48] It is, therefore, supposed that the Au nanoclusters are formed in such a nucleation site. As has been found out, GC is a porous material and pores 1.6–2.5 nm in diameter exist.[49] The pore size depends mainly on the thermal treatment and is larger the higher the annealing temperature.[49] The GC-30 used in the present work was prepared at 3000 °C, the highest temperature for the thermal treatment, and is expected to have the largest pores. Moreover, no significant change in pore size and its distribution was observed after 360 MeV Xe irradiation as analyzed by small-angle x-ray scattering.[50] This result suggests that the nanometer-sized pores still survive in GC-30 even after Au implantation. If the Au nanocluster of ~1 nm are formed inside pores with a few nanometers in size, the environment is similar to that for Au nanoclusters supported on a carbon substrate. For the Au nanoclusters of 2–3 nm, similar to the size of the pores, their whole surfaces are in contact with a carbon matrix, which diminishes the Coulomb charging on the clusters in a photoemission process and hence reduces the $4f$-binding energy shift.

Recently, Kröger *et al.*[51] measured the $4f$ and $5d$ spectra for Au nanoclusters formed on fullerene surface. Their results clearly differ from the previous ones; for example, for the $5d$ splittings of 1.92 ± 0.20 and 2.38 ± 0.05 eV, the $4f$ shifts in their work were 0.35 ± 0.05 and 0.11 ± 0.05 eV, respectively, much smaller than the semiempirical value (~0.6 and ~0.3 eV, see Fig. 5) deduced from the previous works by DiCenzo *et al.*,[16] Wertheim *et al.*,[20] and Zhang and Sham.[32] We speculate that the Au nanoclusters may be in contact with several fullerene molecules, whose π electrons screen the positive hole in the photoemission process, although such evidence has not been observed yet.

Thus the comparison between the $4f$-binding energy shift and $5d$ splitting may be able to provide information about the surroundings of Au nanoclusters. To clarify this ability of XPS, Au implanted layer should be characterized with XTEM. Such characterization is now in progress. The disintegration and/or deformation of Au nanoclusters by Ar sputtering might be a problem for sizing them in a matrix using XPS. XTEM observation is also required to establish the sizing method using XPS together with sputter etching.

V. CONCLUSIONS

The $4f$-binding energy shift and $5d$ splitting have been simultaneously measured for Au nanoclusters formed by Au implantation into GC. It is found that Au nanoclusters of 0.7–2.5 nm in diameter are formed. Their size depends on the Au concentration and is larger the higher the concentration. The relationship between the $4f$ shift and $5d$ splitting, referred to as $4f$ shift-$5d$ splitting relation, is very similar to the previous results for Au nanoclusters with diameter $\leqslant$1 nm, but deviates significantly for larger clusters of 1.4–2.5 nm in diameter. We interpret this result as follows. The smaller cluster is positively charged in a photoemission process due to insufficient contact with a carbon matrix, while for the larger charged cluster, increased contact area reduces the Coulomb charging. The size-dependent difference in environment around a Au nanocluster leads to the deviation of the $4f$ shift-$5d$ splitting relation from the previous results for well-isolated clusters.

ACKNOWLEDGMENTS

Hans-Gerd Boyen of Universität Ulm and Petra Reinke of University of Virginia are acknowledged for fruitful discussions. This work was performed under the cooperative research program of TIARA of Japan Atomic Energy Agency and IMR of Tohoku University.

[1] R. Ruppin, J. Appl. Phys. **59**, 1355 (1986).
[2] K. L. Kelly, E. Coronado, L. L. Zhao, and G. C. Schatz, J. Phys. Chem. B **107**, 668 (2003).
[3] B. Palpant *et al.*, Phys. Rev. B **57**, 1963 (1998).
[4] G. Medeiros-Ribeiro, D. A. A. Ohlberg, and R. S. Williams, Phys. Rev. B **59**, 1633 (1999).
[5] P. Zhang and T. K. Sham, Appl. Phys. Lett. **81**, 736 (2002).
[6] Y. Li, P. Xiong, S. von Molnár, Y. Ohno, and H. Ohno, Phys. Rev. B **71**, 214425 (2005).
[7] G. L. Zhang, W. H. Liu, F. Xu, and W. Hu, Appl. Phys. Lett. **61**, 2527 (1992).
[8] G. Q. Yu, B. K. Tay, Z. W. Zhao, X. W. Sun, and Y. Q. Fu, Physica E (Amsterdam) **27**, 362 (2005).
[9] S. Charvet, R. Madelon, F. Gourilleau, and R. Rizk, J. Appl. Phys. **85**, 4032 (1999).
[10] H. Mertens, J. Verhoeven, A. Polman, and F. D. Tichelaar, Appl. Phys. Lett. **85**, 1317 (2004).
[11] G. De, L. Tapfer, M. Catalano, G. Battaglin, F. Caccavale, F. Gonella, P. Mazzoldi, and R. F. Haglund, Jr., Appl. Phys. Lett. **68**, 3820 (1996).
[12] B. Samuneva, Y. Dimitrev, V. Dimitrov, E. Kashchieva, and G. Encheva, J. Sol-Gel Sci. Technol. **13**, 969 (1998).
[13] G. Battaglin, A. Boscolo-Boscoletto, P. Mazzoldi, C. Meneghini, and G. W. Arnold, Nucl. Instrum. Methods Phys. Res. B **116**, 527 (1996).
[14] D. Ila, E. K. Williams, S. Sarkisov, C. C. Smith, D. B. Poker, and D. K. Hensley, Nucl. Instrum. Methods Phys. Res. B **141**, 289 (1998).
[15] A. L. Stepanov and I. B. Khaibullin, Rev. Adv. Mater. Sci. **9**, 109 (2005).
[16] S. B. DiCenzo, S. D. Berry, and E. H. Hartford, Jr., Phys. Rev. B **38**, 8465 (1988).
[17] D. M. Cox, W. Eberhardt, P. Fayet, Z. Fu, B. Kessler, R. D. Sherwood, D. Sondericker, and A. Kaldor, Z. Phys. D: At., Mol. Clusters **20**, 385 (1991).
[18] H.-G. Boyen *et al.*, Phys. Rev. Lett. **94**, 016804 (2005).
[19] K. Takahiro *et al.*, Abstracts of International Seminar on Ion-Atom Collisions, ISIAC XVIII, Stockholm, 30 July–1 August 2003 (unpublished), p.

63; Abstracts of the Seventh International Conference on Atomically Controlled Surfaces Interfaces and Nanostructures 2003 (unpublished), p. 600; K. Takahiro, A. Terai, T. Morikawa, K. Kawatsura, S. Yamamoto, and H. Naramoto, JAERI-Review 2004-25, TIARA Annual report 2003, 187 (2004).
[20]G. K. Wertheim, S. B. DiCenzo, and S. E. Youngquist, Phys. Rev. Lett. **51**, 2310 (1983).
[21]M. Quinten, I. Sander, P. Steiner, U. Kreibig, K. Fauth, and G. Schmid, Z. Phys. D: At., Mol. Clusters **20**, 377 (1991).
[22]T. Ohgi and D. Fujita, Phys. Rev. B **66**, 115410 (2002).
[23]A. Howard, D. N. S. Clark, C. E. J. Mitchell, R. G. Egdell, and V. R. Dhanak, Surf. Sci. **518**, 210 (2002).
[24]J. N. O'Shea, M. A. Phillips, M. D. R. Taylor, P. Moriarty, M. Brust, and V. R. Dhanak, Appl. Phys. Lett. **81**, 5039 (2002).
[25]M. Imamura and A. Tanaka, Phys. Rev. B **73**, 125409 (2006).
[26]Y. Baer, P. F. Hedén, J. Hedman, M. Klasson, C. Nordling, and K. Siegbahn, Phys. Scr. **1**, 55 (1970).
[27]S. B. M. Hagström, in *Electron Spectroscopy*, edited by D. A. Shirley (North-Holland, Amsterdam, 1972), p. 515; D. A. Shirley, *ibid.* (North-Holland, Amsterdam, 1972), p. 603.
[28]X. Webster, W. R. Salaneck, and I. A. Aksay, Solid State Commun. **19**, 329 (1976).
[29]S.-T. Lee, G. Apai, M. G. Mason, R. Benbow, and Z. Hurych, Phys. Rev. B **23**, 505 (1981).
[30]W. F. Egelhoff, Jr., J. Vac. Sci. Technol. **20**, 668 (1982).
[31]M. G. Mason, Phys. Rev. B **27**, 748 (1983).
[32]A. Bzowski, T. K. Sham, R. E. Watson, and M. Weinert, Phys. Rev. B **51**, 9979 (1995).
[33]P. Zhang and T. K. Sham, Phys. Rev. Lett. **90**, 245502 (2003).
[34]H. Roulet, J.-M. Mariot, G. Dufour, and C. F. Hague, J. Phys. F: Met. Phys. **10**, 1025 (1980).
[35]B. D. Cullity, *Elements of X-ray Diffraction* (Addison-Wesley, Reading, MA, 1978), p. 284.
[36]J. P. Eberhart, *Structure and Chemical Analysis of Materials* (Wiley, Chichester, 1991), p. 203.
[37]A. Jablonski, Surf. Interface Anal. **23**, 29 (1995).
[38]P. H. Citrin, G. K. Wertheim, and Y. Baer, Phys. Rev. B **27**, 3160 (1983).
[39]T. T. P. Cheung, Surf. Sci. **140**, 151 (1984).
[40]J. F. Ziegler, J. P. Biersack, and U. Littmark, The Stopping and Ranges of Ions in Solids (Pergamon, New York, 1985), and also available from http://www.srim.org/
[41]S. Tamura, C. J. Powell, and D. R. Penn, Surf. Interface Anal. **21**, 165 (1994).
[42]B. Dischler and G. Brandt, IDR, Ind. Diamond Rev. **45**, 131 (1985).
[43]J. J. Hauser, Solid State Commun. **17**, 1577 (1975).
[44]J. Fink, T. Muller-Heinzerling, J. Pfluger, A. Bubenzer, P. Koidl, and G. Crecelius, Solid State Commun. **47**, 687 (1983).
[45]G. M. Jenkins and K. Kawamura, Nature (London) **231**, 175 (1971).
[46]T. Noda, M. Inagaki, and S. Yamada, J. Non-Cryst. Solids **1**, 285 (1969).
[47]T. Yamaguchi, Carbon **1**, 47 (1963).
[48]J. Wong-Leung, E. Nygren, and J. S. Williams, Appl. Phys. Lett. **67**, 416 (1995).
[49]S. Bose and R. H. Bragg, Carbon **19**, 289 (1981).
[50]P. Fratzl, G. Vogl, and S. Klaumünzer, J. Appl. Crystallogr. **24**, 588 (1991).
[51]H. Kröger, P. Reinke, M. Büttner, and P. Oelhafen, J. Chem. Phys. **123**, 114706 (2005).